

A MAJOR X-RAY OUTBURST FROM AN ULTRALUMINOUS X-RAY SOURCE IN M82

PHILIP KAARET¹, HUA FENG^{2,1}, AND MARK GORSKI¹

submitted to ApJ

ABSTRACT

We detected a major X-ray outburst from M82 with a duration of 79 days, an average flux of $5 \times 10^{-11} \text{ erg cm}^{-2} \text{ s}^{-1}$ in the 2-10 keV band, and strong variability. The X-ray spectrum remained hard throughout the outburst. We obtained a Chandra observation during the outburst that shows that the emission arises from the ultraluminous X-ray source X41.4+60. This source has an unabsorbed flux of $(5.4 \pm 0.2) \times 10^{-11} \text{ erg cm}^{-2} \text{ s}^{-1}$ in the 0.3-8 keV band, equivalent to an isotropic luminosity of $8.5 \times 10^{40} \text{ erg s}^{-1}$. The spectrum is adequately fitted with an absorbed power-law with a photon index of 1.55 ± 0.05 . This photon index is very similar to the value of 1.61 ± 0.06 measured previously while the flux was $(2.64 \pm 0.14) \times 10^{-11} \text{ erg cm}^{-2} \text{ s}^{-1}$. Thus, the source appears to remain in the hard state even at the highest flux levels observed. The X-ray spectral and timing data available for X41.4+60 are consistent with the source being in a luminous hard state and a black hole mass in the range of one to a few thousand solar masses.

Subject headings: black hole physics – galaxies: individual: M82 galaxies: stellar content – X-rays: galaxies – X-rays: black holes

1. INTRODUCTION

The bright X-ray sources in external galaxies, known as ultraluminous X-ray sources (ULXs), are of current interest because they represent either an unusual state of mass accretion, not or seldom seen from Galactic stellar-mass black hole X-ray binaries, or binary systems containing intermediate-mass black holes (Colbert & Mushotzky 1999; Makishima et al. 2000). The ULX with the highest observed X-ray flux, CXOU J095550.2+694047 = X41.4+60 (Kaaret et al. 2001), is located in the nearby starburst galaxy M82 at a distance of 3.63 Mpc. If the radiation from X41.4+60 is isotropic and from an accreting object, then the mass of the accretor must be in excess of $500 M_{\odot}$ to avoid violating the Eddington limit. X41.4+60 is offset from the dynamical center of the galaxy (Kaaret et al. 2001), produces quasiperiodic oscillations (QPOs) in the 50–120 mHz range (Strohmayer & Mushotzky 2003; Mucciarelli et al. 2006; Dewangan, Titarchuk, & Griffiths 2006; Feng & Kaaret 2007), produces little if any radio emission (Kaaret, Simet, & Lang 2006b), and exhibits an X-ray periodicity of 62 days (Kaaret, Simet, & Lang 2006a,b; Kaaret & Feng 2007). The position of X41.4+60 is within $1''$ of the position of an infrared source (Kaaret et al. 2004) identified as the super star cluster MGG 11 (McCraday, Gilbert, & Graham 2003) that has an extremely dense core that may have led to numerous stellar collisions and the formation of an intermediate mass black hole (Portegies Zwart et al. 2004).

In on-going monitoring of M82 using the Proportional Counter Array (PCA) on the Rossi X-Ray Timing Explorer (RXTE), we detected a major flare from M82 with a peak flux corresponding to an isotropic luminosity of $1.1 \times 10^{41} \text{ erg s}^{-1}$. After the onset of this remarkable X-

ray flare, we obtained imaging X-ray observations with the Chandra X-Ray Observatory. We describe X-ray observations with RXTE in § 2, with Chandra in § 3, and discuss the results in § 4.

2. RXTE OBSERVATIONS

We monitored M82 using the PCA on RXTE (Bradt, Rothschild, & Swank 1993) under programs 92098 and 93123 (PI Kaaret). As described in Kaaret, Simet, & Lang (2006a,b); Kaaret & Feng (2007), we analyzed the real time data from RXTE soon after the data became available on the RXTE ftp site which enabled us to request a target of opportunity observation with the Chandra X-ray Observatory (Weisskopf et al. 2002) after detection of the flare.

The RXTE results presented here were obtained with the production data and the analysis was carried out with version 6.4.1 of the HEASoft package and the CALDB available in June 2008. After the data were retrieved, they were filtered to select good time intervals such that Proportional Counter Unit (PCU) 2 was on, the source was more than ten degrees above the horizon, the pointing offset from the source was less than 0.01° , the satellite was more than 30 s past the South Atlantic Anomaly (SAA), and the electron contamination was low, specifically with an electron rate less than 0.1 c/s. A background file was made for the same interval as the observation with the model `pca_bkgd_cmfpaint17_eMv20051128.mdl`. The tool `saextrct` was used to make both light curves and spectra for the source and background, using only data from PCU 2. Spectra in the 3-12 keV band were fitted with a power-law model using the spectral fitting program XSPEC to obtain a measurement of the flux in the 2–10 keV band. A power-law model with interstellar absorption with the column density fixed to $1.2 \times 10^{22} \text{ cm}^{-2}$ was used. The average photon index for the observations shown in Fig. 1 was 2.15 with a standard deviation of 0.21. The average uncertainty in the photon index was 0.20, so there is no evidence for spectral variation.

¹ Department of Physics and Astronomy, University of Iowa, Van Allen Hall, Iowa City, IA 52242.

² Department of Engineering Physics and Center for Astrophysics, Tsinghua University, Beijing 100084, China.

Fluxes calculated with the photon index fixed to the average value agree with those calculated from the fits with the photon index left free. We note that the PCA field of view is about 1° FWHM. Thus, the PCA spectra represent the summed spectra of all the sources in M82 and not the spectrum of the X41.4+60 alone; the spectral index measured with the PCA is not expected to agree with that measured for X41.4+60 alone with Chandra. We have reduced the PCA fluxes by a factor of 1.18 because the PCA calibration appears to give systematically higher fluxes than previous and other current X-ray instruments (Tomsick et al. 1999).

Fig. 1 shows the observed flux in the 2–10 keV band versus time from spectral fits with the photon index fixed to 2.15. The X-ray flare begins at MJD 54247.2 when the flux rises above $5 \times 10^{-11} \text{ erg cm}^{-2} \text{ s}^{-1}$. The flux remains high, although highly variable, until MJD 54325.7. After that date, the flux returns to the usual range for M82 of $\sim 2 - 3 \times 10^{-11} \text{ erg cm}^{-2} \text{ s}^{-1}$. The flare duration was 79 days. The peak flux was $6.1 \times 10^{-11} \text{ erg cm}^{-2} \text{ s}^{-1}$, the average flux was $4.6 \times 10^{-11} \text{ erg cm}^{-2} \text{ s}^{-1}$, and the root-mean-square (rms) variation in the flux was $9.7 \times 10^{-12} \text{ erg cm}^{-2} \text{ s}^{-1}$ indicating an rms amplitude of 21%. The duration of the flare is similar to that of the flare found by Rephaeli & Gruber (2002). The level of variability is higher, but that may, at least in part, be due to the limited coverage (only four observations) available to Rephaeli & Gruber (2002).

Fig. 2 shows a hardness-intensity diagram for M82. We chose energy bands similar to those used by Belloni et al. (2005) in order to facilitate comparison with previous results. Specifically, we used the count rate in the 3.6–21.6 keV band as the measure of intensity and the ratio of counts in the 6.5–11.0 keV band to those in the 3.6–6.5 keV band as the measure of hardness. The plot includes those observations shown in Fig. 1 for which the hardness could be calculated to a fractional accuracy of better than 0.15. The photons recorded by the PCA include diffuse emission and other X-ray sources in M82 that affect the intensity and hardness. However, the changes in intensity and hardness are likely dominated by X41.4+60. Fig. 2 indicates that X41.4+60 is usually in the hard state and remains in the hard state during the whole of the outburst. There is no significant change in hardness as the intensity changes over a factor of about 4.

We searched for rapid variability following the procedures described in Kaaret & Feng (2007). No statistically significant quasiperiodic oscillations (QPOs) were found. This may be because the new RXTE observations are rather short, typically less than 1000 s, and have fewer Proportional Counter Units turned on compared to previous RXTE observations in which QPOs were detected.

3. OBSERVATIONS AND RESULTS

After detection of a high X-ray flux level with the PCA, a Chandra (Weisskopf et al. 2002) Target of Opportunity Observation (TOO) was triggered. The observation (ObsID 8190; PI Kaaret) began on 2007 June 2 at 02:41:29 UT (MJD 54253.112). The observation was made using the Advanced CCD Imaging Spectrometer spectroscopy array (ACIS-S) and the High Resolution Mirror Assembly (HRMA). We obtained 52,768 s of useful exposure.

The ACIS-S was used in imaging mode. As described in Kaaret, Simet, & Lang (2006b) for our previous TOO, we attempted to reduce pile-up by offsetting the target $-3'57$ along the Y-detector coordinate in order to image the source using a point spread function that spread the beam over many CCD pixels and operating only the S3 chip in the 1/8 sub-array mode to reduce the frame time to 0.441 s. We also re-analyzed the Chandra observation (ObsID 6097) of M82 that began on 2005 February 4 at 23:34:40 UT (MJD 53405.982).

The Chandra data were subjected to standard data processing and event screening (Ciao version 4.0.1 using CALDB version 3.4.3). Neither observation showed any strong background flares. Following Kaaret, Simet, & Lang (2006b), we constructed images for the 2–8 keV band and used the *wavdetect* tool to locate the X-ray sources. Fig. 3 shows the images and the source regions for X41.4+60 defined using the 2–8 keV band. Note that the sources appear elongated because they are off axis. The ellipses encompassing X41.4+60 have semi-major axes of $5.69''$ and $7.11''$, and semi-minor axes of $3.33''$ and $2.93''$, respectively for observation 6097 and 8190. The background region is defined by a $8.49''$ by $3.81''$ box placed near the source, but avoiding other point sources and the readout streak for X41.4+60. In observation 8190, some photons from another bright source, X42.3+59, fall into the region defined for X41.4+60. When accumulating the spectrum for X41.4+60, we excluded photons from the region around X42.3+59, indicated by the dotted ellipse in Fig. 3, in order to minimize the contamination. Response matrices were calculated using *mkacisrmf* and the spectra were fitted using XSPEC 12 which is part of the HEASoft package.

We estimated the pileup in the spectrum for each observation by summing the counts (with no energy selection) in a 3×3 pixel box around the pixel with the maximum number of counts and then calculating the counts per frame within the box. Observation 6097 yielded 0.18 counts/frame and observation 8190 yielded 0.31 counts/frame. Thus, within the central 3×3 pixel box, the fraction of piled-up events is 5.2% for observation 6097 and 10.3% for observation 8190. The central 3×3 pixel box contains 40% and 38% of the total events, so the overall pile-up fraction is about 2% and 4%, respectively for observation 6097 and 8190.

Even though the overall pile-up is low, the central regions of the image in the second observation are strongly affected by pile-up. We chose to use two methods to model the pile-up. The first was to use the ACIS pile-up model in XSPEC version 12.4.0x. We fitted the spectral data in the 0.3–8 keV band with an absorbed power law with and without the pileup model. The pileup model parameters were set to match the frame time of the Chandra observations. Since the observation is off-axis, the fraction of photons in the piled-up part of the spectrum is different from the 95% for an on-axis point source. We set this fraction (the parameter *psfrac*) to the ratio of counts, with no energy selection, in the 3×3 pixel box around the pixel with the maximum number of counts to the total counts in the source extraction region. The values are 0.40 and 0.38 for observations 6097 and 8190, respectively. The alpha values from the best fits are 0.33 for observation 6097 and 0.25 for observation 8190.

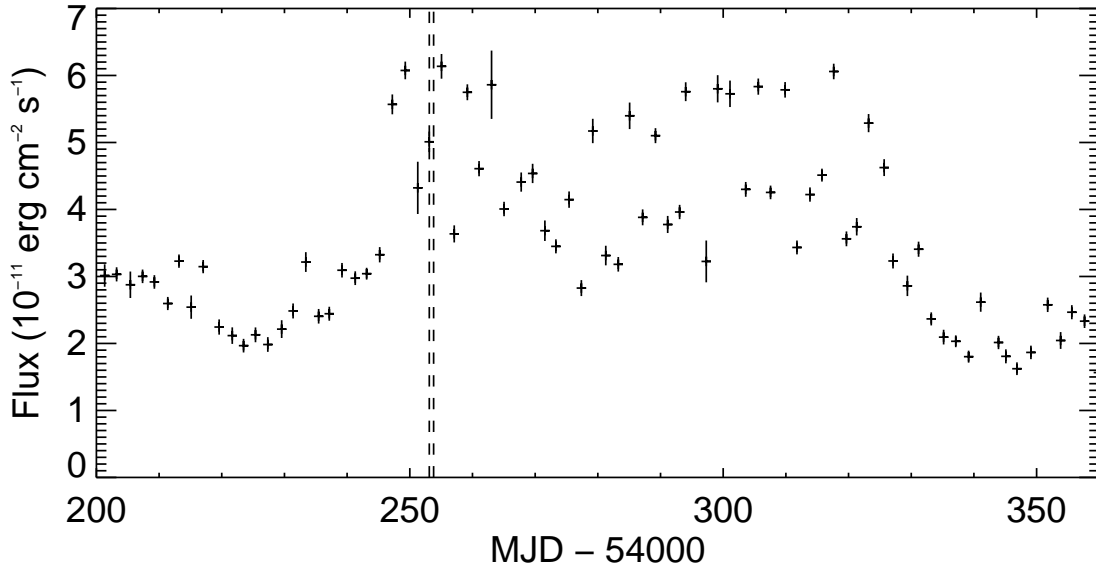


FIG. 1.— Light curve of M82 obtained using the PCA on RXTE. The plot shows the flux in the 2–10 keV band calculated for each observation versus the observation date in MJD. The vertical dashed lines indicate the time of the Chandra observation. An X-ray outburst occurred from MJD 54247 to MJD 54326.

TABLE 1
X-RAY SPECTRAL FITS

	Γ	N_H (10^{22} cm^{-2})	Flux ($10^{-11} \text{ erg cm}^{-2} \text{ s}^{-1}$)	χ^2/DoF
Observation 6097 - 2005 February 4				
MARX input	1.61	1.15	1.55	
MARX output	1.65 ± 0.03	1.20 ± 0.03	1.27 ± 0.05	433.2/401
" pileup	1.73 ± 0.05	1.24 ± 0.03	1.30 ± 0.06	421.7/400
Data	1.63 ± 0.03	1.18 ± 0.03	1.29 ± 0.05	347.1/407
" pileup	1.67 ± 0.05	1.20 ± 0.03	1.30 ± 0.07	343.1/406
Observation 8190 - 2007 June 2				
MARX input	1.55	1.29	3.20	
MARX output	1.50 ± 0.02	1.32 ± 0.02	2.67 ± 0.08	596.6/456
" pileup	1.63 ± 0.04	1.39 ± 0.03	2.77 ± 0.11	533.9/455
Data	1.50 ± 0.02	1.31 ± 0.02	2.66 ± 0.08	587.8/463
" pileup	1.56 ± 0.03	1.34 ± 0.03	2.70 ± 0.11	575.2/462

NOTE. — The table includes for both observations: the parameters input to the Marx, the best fitted parameters for fits of an absorbed power-law model and an absorbed power-law model with pile-up correction fitted to the output of the Marx simulation and to the data. The columns give: Γ - the photon index, N_H - the absorption column density, Flux - absorbed source flux in the 0.3–10 keV band; and the χ^2 and number of degrees of freedom in the fit.

To check the modeling of the pileup, the observations were simulated using Marx version 4.3.0. The Marx program is designed to simulate a Chandra observation. We set up simulations matching the off-axis pointing and roll angle for each observation. We followed an iterative process to find input parameters to Marx that best matched the data: we assumed a set of input parameters for an absorbed power-law model (absorption column density, photon index, and normalization), ran Marx using those parameters, fitted the output from Marx using an absorbed power-law model, and then compared those best fitted parameters to those obtained from the data. Because of the high source flux, the parameters extracted from fits to the Marx simulation without the pile-up model differ significantly from the input parameters due to the effects of pile-up even the off-axis pointing and the use of a 1/8th sub-array. We then adjusted the input parameters to Marx and repeated the procedure until a good match was obtained between the fits to the output of the simulation and the data.

The final set of parameters input to the Marx simulation, the results of the fits to output of that simulation, and the results of the fit to the data are presented in Table 1. We take the input to the Marx simulations as our best estimate of the true source properties. Comparing the Marx inputs with the fits to the data using the power-law model with pile-up correction provide an indication of the level of systematic uncertainty in the modeling. Our best estimate of the photon index is 1.61 ± 0.06 for observation 6097 and 1.55 ± 0.05 for 8190. The absorption-corrected flux in the 0.3–8 keV band in units of $10^{-11} \text{ erg cm}^{-2} \text{ s}^{-1}$ is 2.64 ± 0.14 for the first observation, and 5.4 ± 0.2 for the second. In the 2–10 keV band, the absorption-corrected fluxes are 1.86 ± 0.10 and 4.0 ± 0.2 in the same units. Thus, the photon index remained constant, within the uncertainties, while the flux changed by a factor of 2. We note that Berghea et al. (2008) reported an unusually hard spectrum for X41.4+60 for an observation on 1999 December 30, but this observation is strongly affected by pile-up

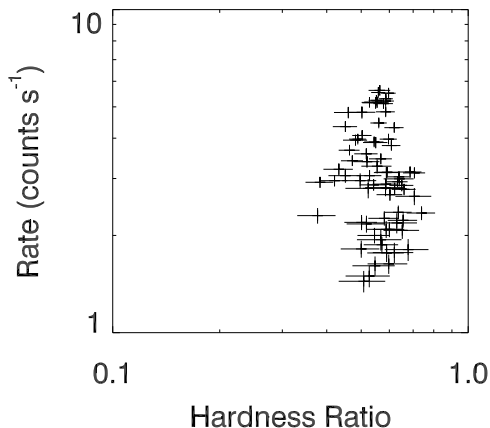


FIG. 2.— Hardness-intensity diagram of M82 obtained using the PCA on RXTE. The plot shows the count rate in the 3.6–21.6 keV band as a function of the hardness, defined as the ratio of counts in the 6.5–11.0 keV band to those in the 3.6–6.5 keV band. The plot includes those observations shown in Fig. 1 for which the hardness could be calculated to a fractional accuracy of better than 0.15. The source remained in the hard state for the whole outburst.

with a pile fraction of at least 17% in the peak 3×3 pixel box.

The spectra of some ULXs appear to have curvature at high energies, around 5 keV and above (Feng & Kaaret 2005; Stobbart et al. 2006; Roberts 2007), and it is of interest to search for spectral curvature from X41.4+60. Unfortunately, the PCA observations around the time of the Chandra observation are too short to make a useful measurement of the high energy extension of the spectrum. Also, as noted above, the PCA field of view is larger than the angular size of M82, so the PCA spectrum would not reflect that of X41.4+60 alone.

We fitted the Chandra data for observation 8190 using various models with pile-up and interstellar absorption. We fixed the alpha parameter to the value found in the single power-law fit as this was necessary to prevent alpha from being driven to 1.0 (in which case all piled-up photons are accepted as valid, negating the pile-up correction). A Comptonization model, `comptt` in XSPEC, provided no improvement in the fit over the power-law model and the best fit temperature was well above 8 keV. An exponentially cutoff power-law model, `cutoffpl`, gave a cutoff energy larger than 8 keV, i.e. above the Chandra band. A multicolor disk blackbody model provides a substantially worse fit than the simple power-law model. A multicolor disk blackbody model in which the temperature varies with radius as r^{-p} , the `diskpbb`, provided an adequate fit with $p = 0.57 \pm 0.01$ and an inner disk temperature of $6.5^{+1.3}_{-0.8}$ keV. However, difficulties with the physical interpretation of this model given the high apparent luminosity and high temperature needed for X41.4+60 have already been raised by Miyakawa et al. (2008) based on spectral fitting with Suzaku. They conclude that the model is physically untenable and that the source appears to be in the power-law state. We find an even higher temperature than Miyakawa et al. (2008) which would exacerbate the problems.

Fig. 5 shows light curves of X41.4+60 in the 0.3–2 keV and 2–8 keV bands for the 2007 observation. The same source region used to extract the spectrum was used to extract the light curve. The time bin size is 2048 times the CCD frame time, i.e. 903.2 s. No attempt was made to correct for pile-up. The source was variable on time

scales of thousands of seconds in the 2–8 keV band, but remained relatively constant in the 0.3–2 keV band. We divided the data into high count rate and low count rate halves and fitted the spectra for each using an absorbed power-law model with pile-up correction. The absorption column density is consistent, within errors, while the photon index for the high count rate part, $\Gamma = 1.52 \pm 0.03$, is somewhat harder than for the low count rate part, $\Gamma = 1.63 \pm 0.04$. This would favor spectral pivoting as the origin of the variability.

4. DISCUSSION

The observed flux of X41.4+60 measured with Chandra on 2007 June 2 is $3.0 \times 10^{-11} \text{ erg cm}^{-2} \text{ s}^{-1}$ in the 2–10 keV band. The flux from the remainder of M82 is $1.8 \times 10^{-11} \text{ erg cm}^{-2} \text{ s}^{-1}$. The flux of the whole galaxy as measured by the PCA just before the start of the Chandra observation was $(5.0 \pm 0.2) \times 10^{-11} \text{ erg cm}^{-2} \text{ s}^{-1}$ which is in agreement. We adopt $1.8 \times 10^{-11} \text{ erg cm}^{-2} \text{ s}^{-1}$ as an estimate of the flux arising from sources other than X41.4+60 in M82 for the PCA observations. Then, the peak observed flux in the 2–10 keV band from X41.4+60 during the outburst is $4.3 \times 10^{-11} \text{ erg cm}^{-2} \text{ s}^{-1}$ and the average flux is $2.8 \times 10^{-11} \text{ erg cm}^{-2} \text{ s}^{-1}$. Assuming isotropic emission from a source located in M82 and converting these absorbed fluxes into intrinsic fluxes using the Chandra spectrum derived above, the peak luminosity in the 2–10 keV band is $7.6 \times 10^{40} \text{ erg s}^{-1}$, the average luminosity is $4.9 \times 10^{40} \text{ erg s}^{-1}$, and the total energy released in the outburst is $\sim 3 \times 10^{47} \text{ erg}$. Extending the energy band to the full band, 0.3–12 keV, detected from X41.4+60 during the outburst would increase these values by 70%.

Remillard & McClintock (2006) have identified three main spectral/timing states of stellar-mass black hole X-ray binaries (BHXBs): the steep power-law state, the thermal dominant state, and the hard state. The Chandra spectra show that X41.4+60 is quite hard during both observations with a photon index near 1.6. While it is not possible to rule out spectral curvature above 8 keV, the observed 0.3–8 keV Chandra spectra are inconsistent with those observed for BHXBs in the steep power-law state or thermal dominant states. The Chandra spectra of X41.4+60 are adequately described by a single power-law with a photon index of $\Gamma = 1.6$ and are consistent with identification of the source as being in the hard state – defined as having a spectrum dominated by a power-law component with 80% or more of the total flux and a photon index $1.4 < \Gamma < 2.1$, and pronounced continuum timing noise with an integrated rms power greater than 10%. We note that the photon index at energies below any break or cutoff in the power-law component is used by Remillard & McClintock (2006) for the state classifications. Thus, identification of X41.4+60 as in the hard state is robust, even if the spectrum shows curvature at higher energies.

The spectrum remains hard when the flux increases to the brightest levels ever seen from the source. The Chandra data show that the source is variable during the second observation, but are inadequate to detect fast timing noise. An XMM-Newton observation made on 2004 April 21 reveals broad band timing noise (Dewangan, Titarchuk, & Griffiths 2006; Mucciarelli et al. 2006) which appears to arise from

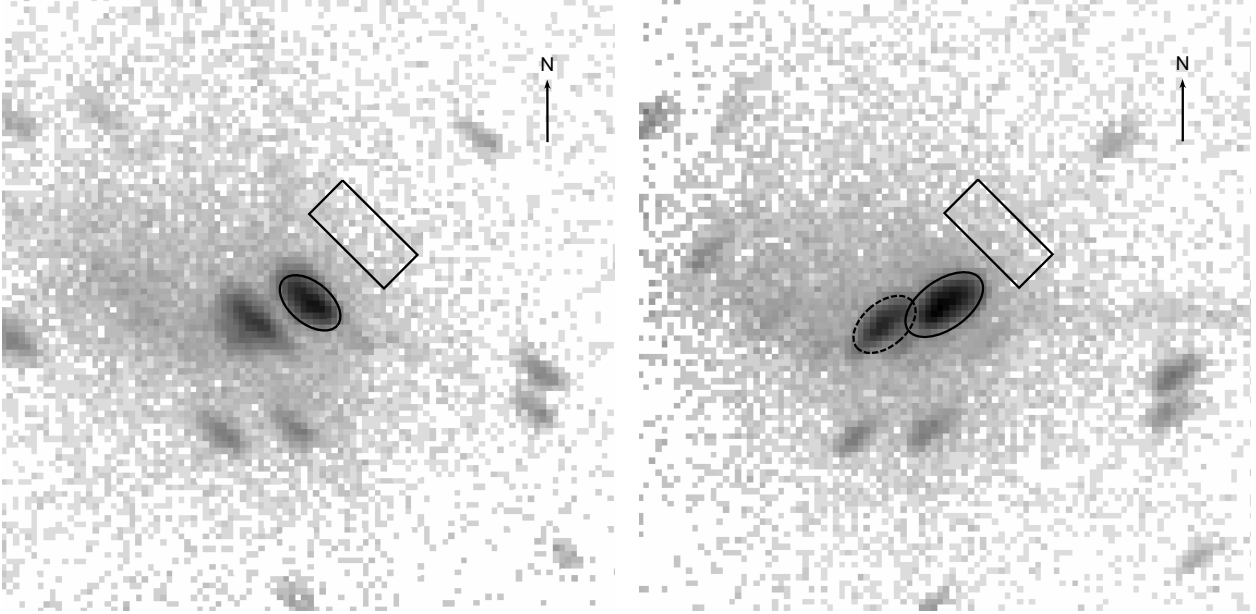


FIG. 3.— X-ray images of M82 in the 2–8 keV band. The panel on the left shows the Chandra observation on 2005 February 4, while the panel on the right shows the new Chandra observation on 2007 June 2. The intensity scale is the same in the two images. In both panels, the solid ellipse shows the source extraction region, the rectangle is the background region, and the arrow points North and has a length of $5''$. For the 2007 observation, the dashed ellipse shows the source region for the X-ray source X42.3+59. This region was excluded in the extraction of photons from X41.4+60.

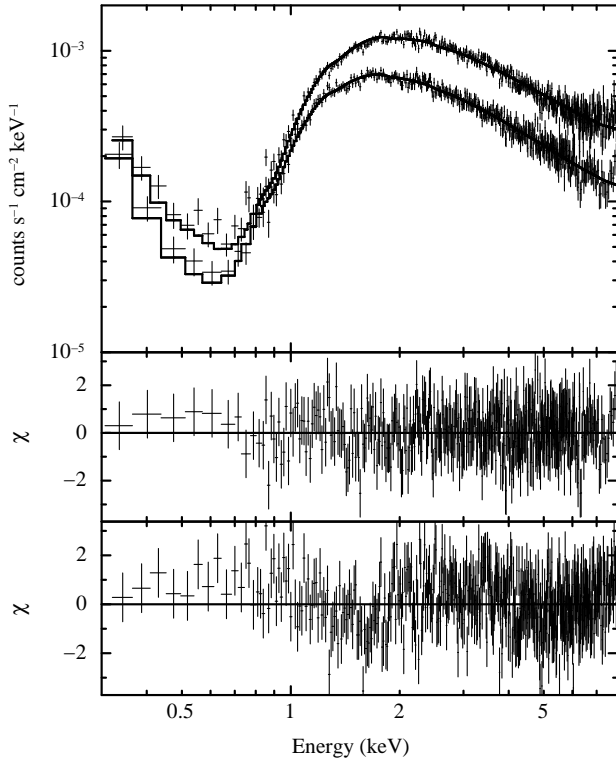


FIG. 4.— Energy spectrum of X41.4+60. The top panel shows the counts $\text{cm}^{-2} \text{s}^{-1} \text{keV}^{-1}$ for both observations on the same scale. Observation 8190 is the upper curve at all energies. The middle panel shows the residuals of the fit for observation 6097. The bottom panel shows the residuals for observation 8190. The spectral shape at high energies is very similar between the two observations. The column density for observation 8190 is slightly higher than for observation 6097.

X41.4+60 (Feng & Kaaret 2007). The integrated power in the 6–80 mHz range is near 17%. This value is consistent with the magnitude of the rms power required for a source to be in the hard state, but the frequency

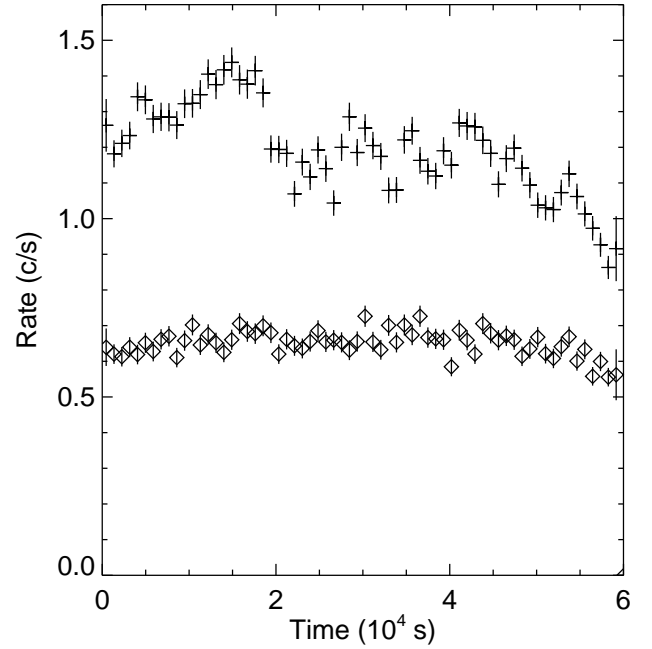


FIG. 5.— Light curves of X41.4+60 in the 2–8 keV band (crosses) and the 0.3–2 keV band (diamonds) for the 2007 observation. The source was strongly variable in the 2–8 keV band.

band is shifted relative to the 0.1–10 Hz band used by Remillard & McClintock (2006).

The PCA data show that X41.4+60 remains in the hard state during the whole of the outburst, see Fig 2. There is no significant change in hardness as the intensity changes over a factor of about 4. This lack of change in hardness is similar to the evolution of GX 339–4 in the rising phase of its 2002/3 outburst (Belloni et al. 2005). This behavior suggests that the mass accretion rate in X41.4+60 never becomes high enough at any point during the outburst to push the system out of the hard state.

Stellar-mass black hole X-ray binaries have been ob-

served to remain in the hard state at luminosities as high as $L/L_E \sim 0.3$ for GX 339-4 (Zdziarski et al. 2004; Miyakawa et al. 2008) and as high as $L/L_E \sim 0.1$ for XTE J1550-564 (Rodríguez, Corbel, & Tomsick 2003; Yuan et al. 2007), where L is the source luminosity and L_E is the Eddington luminosity. Above this luminosity, the sources transition to a softer spectral state. Assuming that the same limit of $L/L_E < 0.3$ applies to more massive black holes found in the hard state, then the 0.3–8 keV flux measured with Chandra would imply a mass in excess of $2000 M_\odot$ if the object is radiating isotropically. Converting the peak flux observed with RXTE to a 0.3–20 keV luminosity of $1.6 \times 10^{41} \text{ erg s}^{-1}$ would imply a black hole mass in excess of $4000 M_\odot$. Allowing for moderate beaming (note that a geometrically thin accretion disk has a beaming factor of 2 when viewed on axis), could reduce these values by a factor of a few.

Using the correlation between X-ray spectral shape and L/L_E found by Shemmer et al. (2008) for radio-quiet active galactic nuclei (AGN), the photon index of $\Gamma = 1.6$ would suggest that $L/L_E \approx 0.1$. The highest luminosity measured with Chandra would then imply a mass of about $7000 M_\odot$. However, mass estimation via Γ and L_X is only accurate within a factor of about 3 (Shemmer et al. 2008).

Quasi-periodic oscillations have been detected from the central region of M82 (Strohmayer & Mushotzky 2003; Mucciarelli et al. 2006; Dewangan, Titarchuk, & Griffiths 2006) and were localized to X41.4+60 (Feng & Kaaret 2007). The strength and coherence of the QPOs suggests they are of ‘type C’ as defined for stellar-mass black hole X-ray binaries (Remillard & McClintock 2006). Type C QPOs occur in the hard and intermediate states. Thus, the detected QPOs are consistent with the assertion that X41.4+60 remains in the hard state.

Estimation of a precise compact object mass using the QPO frequencies alone is uncertain since the QPO frequencies for individual stellar-mass black holes are known to vary by large factors, but the QPO frequencies can be used to place bounds on the allowed range of masses. Comparing the maximum QPO frequency of 0.113 Hz observed from X41.4+60 with XMM-Newton to the highest observed QPOs frequencies for GRO J1655-40, GRS 1915+105, and XTE J1550-564 (Remillard & McClintock 2006) by scaling mass linearly with QPO frequency, leads to an upper bound on the compact object mass of $2.7 \times 10^4 M_\odot$. If the QPO from X41.4+60 is identified as a low frequency QPO, then a similar comparison with the highest observed low frequency QPOs for the same stellar-mass black hole binaries (McClintock & Remillard 2006) suggests an upper bound of $1700 M_\odot$. We note that the ratio of the QPO frequency to the frequency of the break in the broadband timing noise of X41.4+60 is consistent with that seen for low frequency QPOs. This, and the fact that strong high frequency QPOs are seen only in the steep power-law state of stellar mass black holes while low frequency QPOs are seen in the hard state, suggests that the QPOs from X41.4+60 are analogous to low frequency QPOs.

Better mass constraints may be obtained by combining spectral and timing information. We note that several authors have used XMM-Newton data to infer

the spectral shape of X41.4+60. This is unreliable since X42.3+59 contributes significant flux is not resolved from X41.4+60 with XMM-Newton. Thus, all previous work suggesting the presence of a thermal component in the spectrum or identification of the source as being in the steep power-law or intermediate state must be re-visited (Strohmayer & Mushotzky 2003; Fiorito & Titarchuk 2004; Mucciarelli et al. 2006; Dewangan, Titarchuk, & Griffiths 2006; Okajima, Ebisawa, & Kawaguchi 2006; Casella et al. 2008). Simultaneous timing and spectral measurements of X41.4+60 will require simultaneous observations with XMM-Newton and Chandra.

Accreting black holes of all masses are known to produce radio emission while in the hard state. The radio emission, X-ray emission, and black hole mass are related via the ‘fundamental plane’ (Merloni, Heinz, & Di Matteo 2003). As noted in Kaaret et al. (2001), there was a radio transient in 1981 close to the position of X41.4+60, but no radio emission has been detected subsequently. Kaaret, Simet, & Lang (2006b) place an upper limit on the radio flux of 0.7 mJy at 8.5 GHz on 2005 February 3, just before the Chandra observation giving a 2–10 keV luminosity of $3 \times 10^{40} \text{ erg s}^{-1}$. Paragi, Garrett, Biggs (2006) place an upper limit of 67 μJy at 1.6 GHz on 2005 October 27, but, unfortunately, there is no contemporaneous X-ray observation. For upper limits on the radio fluxes, the ‘fundamental plane’ relation can be re-cast to place an upper limit on the black hole mass:

$$M \lesssim 2000 M_\odot \left(\frac{F}{100 \mu\text{Jy}} \right)^{1.28} \left(\frac{L_X}{10^{40} \text{ erg/s}} \right)^{-0.77} \left(\frac{d}{3.6 \text{ Mpc}} \right)^{2.56}$$

where M is the black hole mass, F is the flux at 5 GHz, L_X is the luminosity in the 2–10 keV band, and d is the distance. From the 2005 February data, the limit is $M \lesssim 10^4 M_\odot$. Because there is no X-ray information available for 2005 October, any limit is less secure. Assuming an X-ray luminosity of $1 \times 10^{40} \text{ erg s}^{-1}$, would imply a limit of $M \lesssim 1200 M_\odot$. The scatter in the fundamental plane is significant, about a factor of 10, so the limits from the above equation are uncertain by at least a factor of 3. However, simultaneous X-ray and sensitive radio observations may provide a means to constrain the mass of X41.4+60.

There are several other known ULXs with luminosities near $10^{41} \text{ erg s}^{-1}$ (Gao et al. 2003; Wolter et al. 2006; Miniutti et al. 2006). All of these sources have hard spectra and are, together with X41.4+60, perhaps the best candidates for X-ray detected intermediate-mass black holes (Roberts 2007). Unfortunately, due to the large distances to most of these hyper luminous sources, detailed spectral information and information on any spectral changes correlated with luminosity is limited. This trend toward hard spectra appears to continue down to luminosities around $10^{40} \text{ erg s}^{-1}$ (Feng & Kaaret 2006; Soria et al. 2007; Berghea et al. 2008). For sources with multiple observations, particularly X-16 and X-11 in the Antennae (Feng & Kaaret 2006) and the ULX in NGC 1365 (Soria et al. 2007), the sources appear to remain in the hard state even when the flux changes by factors of several. This suggests that these objects also remain in the hard state. This is evidence against the suggestion

that these sources are stellar-mass black hole X-ray binaries that enter an “ultraluminous branch” of the very high or steep power-law state at high luminosities, since a transition out of this state would be expected at lower luminosities.

We acknowledge partial support from Chandra grant CXC GO7-8085X and NASA Grant NNX08AJ26G. PK acknowledges support from a University of Iowa Faculty Scholar Award.

Facilities: CXO (HRMA, ACIS), RXTE (PCA)

REFERENCES

- Belloni, T., Homan, J., Casella, P., van der Klis, M., Nespoli, E., Lewin, W.H.G., Miller, J.M., Mendez, M. 2005, *A&A*, 440, 207
- Berghea, C.T., Weaver, K.A., Colbert, E.J.M., Roberts, T.P. 2008, *ApJ* to appear, arXiv:0807.1547
- Bradt, H.V., Rothschild, R.E., & Swank, J.H. 1993, *A&AS*, 97, 355
- Casella, P., Ponti, G., Patruno, A., Belloni, T., Miniutti, G., Zampieri, L. 2008, *MNRAS*, 387, 1707
- Colbert, E.J.M. & Mushotzky, R.F. 1999, *ApJ*, 519, 89
- Dewanagan, G.C. Titarchuk, L., Griffiths, R.E. 2006, *ApJ*, 637, L21
- Feng, H. & Kaaret, P. 2005, *ApJ*, 633, 1052
- Feng, H. & Kaaret, P. 2006, *ApJ*, 653, 536
- Feng, H. & Kaaret, P. 2007, *ApJ*, 668, 941
- Fiorito, R. & Titarchuk, L. 2004, *ApJ*, 614, L113
- Gao, Y., Wang, Q.D., Appleton, P.N., Lucas, R.A. 2003, *ApJ*, 596, L171
- Kaaret, P. et al. 2001, *MNRAS*, 321, L29
- Kaaret, P., Alonso-Herrero, A., Gallagher, J.S. III, Fabbiano, G., Zezas, A., Rieke, M.J. 2004, *MNRAS*, 348, L28
- Kaaret, P., Simet, M.G., Lang, C.C. 2006, *Science*, 311, 491
- Kaaret, P., Simet, M.G., Lang, C.C. 2006, *ApJ*, 646, 174
- Kaaret, P. & Feng, H. 2007, *ApJ*, 669, 106
- Makishima, K. et al. 2000, *ApJ*, 535, 632
- McClintock, J.E. & Remillard, R.A. 2006, in *Compact Stellar X-Ray Sources*, ed. W.H.G. Lewin, M. van der Klis, pp. 157-214, Cambridge: Cambridge University Press
- McCrady, N., Gilbert, A.M., Graham, J.R. 2003, *ApJ*, 596, 240
- Merloni, A., Heinz, S., Di Matteo, T. 2003, *MNRAS*, 345, 1057
- Miniutti, G., Ponti, G., Dadina, M., Cappi, M., Malaguti, G., Fabian, A.C., Gandhi, P. 2006, *MNRAS*, 373, L1
- Miyakawa, T., Yamaoka, K., Homan, J., Saito, K., Dotani, T., Yoshida, A., Inoue, H. 2008, *PASJ*, 60, 637
- Mucciarelli, P., Casella, P., Belloni, T., Zampieri, L., Ranalli, P. 2006, *MNRAS*, 365, 1123
- Okajima, T., Ebisawa, K., Kawaguchi, T. 2006, *ApJ*, 652, L105
- Paragi, Z., Garrett, M.A., & Biggs, A.D. 2006, in *The 8th European VLBI Network Symposium*, Torun, Poland, PoS(8thEVN)016
- Portegies Zwart, S.F., Baumgardt, H., Hut, P., Makino, J., McMillan, S. L. W. 2004, *Nature* 428, 724
- Remillard, R.A. & McClintock, J.E. 2006, *ARA&A*, 44, 49
- Rephaeli, Y. & Gruber, D. 2002, *A&A*, 389, 752
- Roberts, T.P. 2007, *ApSS*, 311, 203
- Rodriguez, J., Corbel, S., Tomsick, J.A. 2003, *ApJ*, 595, 1032
- Shemmer, O., Brandt, W.N., Netzer, H., Maiolino, R., Kaspi, S. 2008, *ApJ*, 682, 81
- Soria, R., Baldi, A., Risaliti, G., Fabbiano, G., King, A., La Parola, V., Zezas, A. 2007, *MNRAS*, 379, 1313
- Stobart, A.-M., Roberts, T.P., Wilms, J. 2006, *MNRAS*, 368, 397
- Strohmayer, T.E. & Mushotzky, R.F. 2003, *ApJ*, 586, L61
- Tomsick, J.A., Kaaret, P., Kroeger, R.A., Remillard, R.A. 1999, *ApJ*, 512, 892
- Weisskopf, M.C., Brinkman, B., Canizares, C., Garmire, G., Murray, S., Van Speybrock, L.P. 2002, *PASP*, 114, 1
- Wolter, A., Trinchieri, G., Colpi, M. 2006, *MNRAS* 373, 1637
- Yuan, F., Zdziarski, A. A., Xue, Y., Wu, X.-B. 2007, *ApJ*, 659, 541
- Zdziarski, A. A., Gierliński, M., Mikołajewska, J., Wardziński, G., Smith, D.M., Harmon, B.A., Kitamoto, S. 2004, *MNRAS*, 351, 791